Universidad Tecnológica Nacional
MAYO - AGOSTO 2025 / Año 23 - Nº 53

Revista Tecnología y Ciencia
DOI: https://doi.org/10.33414/rtyc.53.95-108.2025 - ISSN 1666-6933

DFT+U study of structural and electronic properties in $La_{0.12}Sr_{0.88}TiO_3$: implications for solid oxide fuel cell

Estudio DFT+U de las propiedades estructurales y electrónicas del $La_{0.12}Sr_{0.88}TiO_3$: implicaciones para las celdas de combustible de óxido solido

Presentación: 28/04/2025

Aprobación: 06/08/2025

Publicación: 14/08/2025

Ernesto Tagarelli
Departamento Caracterización de Materiales-Gerencia de Investigación Aplicada-Instituto de Nanociencias y Nanomateriales, Centro Atómico Bariloche, Comisión Nacional de Energía Atómica, Argentina.
Universidad Tecnológica Nacional, Facultad Regional La Plata, Argentina.
ernestotagarelli@gmail.com

Jesús Vega-Castillo
Consejo Nacional de Investigaciones Científicas y Técnicas, Argentina.
YPF-Tecnología, Argentina.
jesus.e.vegacastillo@set.ypf.com

Mariela Ortíz
Instituto de Investigaciones Fisicoquímicas Teóricas y Aplicadas, Facultad de Ciencias Exactas Universidad Nacional de la Plata, CONICET, Argentina.
Universidad Tecnológica Nacional, Facultad Regional La Plata, Centro de Investigación y Desarrollo en Ciencia y Tecnología de Materiales, Argentina.
mariela.ortiz@yahoo.com.ar

Alejandra Montenegro-Hernández
Departamento Caracterización de Materiales - Gerencia de Investigación Aplicada - Instituto de Nanociencias y Nanomateriales, Centro Atómico Bariloche, Comisión Nacional de Energía Atómica, Argentina.
Consejo Nacional de Investigaciones Científicas y Técnicas, Argentina
Alejandra.montenegro@gmail.com

Revista Tecnología y Ciencia
DOI: https://doi.org/10.33414/rtyc.53.95-108.2025 - ISSN 1666-6933

Abstract

The results of comparative calculations for bulk properties and electronic structure of the $SrTiO_3$ (STO) perovskite compound and STO doped with lanthanum $La_{0.12}Sr_{0.88}TiO_3$ (LST-12) are discussed using the ab initio density functional theory (DFT). Furthermore, a comprehensive study of the electronic structure of LST-12 with spin polarization configuration was performed. A full Bader charge analysis was employed to study the charge distributions associated with each ion. Finally, on a 4x2x2 supercell of $La_{0.125}Sr_{0.875}TiO_{3-\delta}$ an oxygen vacancy-site was introduced to elucidate the effect on the electronic and structural properties.

Keywords: SOFC, anode, DFT, Bader, vacancy.

Resumen

Este trabajo presenta un estudio comparativo de las propiedades estructurales y la estructura electrónica de la perovskita $SrTiO_3$ (STO) y su variante dopada con lantano, $La_{0,12}Sr_{0,88}TiO_3$ (LST-12), utilizando cálculos por primeros principios basados en la teoría del funcional de la densidad (DFT). En el compuesto LST-12, se realizó un análisis detallado de la estructura electrónica utilizando una configuración con polarización de espín. Además, se examinó la distribución de carga asociada a cada ion mediante un análisis de carga de Bader. Finalmente, se introdujo una vacancia de oxígeno en una supercelda 4×2×2 de $La_{0.125}Sr_{0.875}TiO_{3-\delta}$ para evaluar su impacto en las propiedades del material.

Palabras clave: SOFC, ánodo, DFT, Bader, vacancias.

Introduction

Solid oxide fuel cells (SOFCs) are considered as one of the most efficient and environmental-friendly technologies to address some of challenges that energy industry is currently facing. The main advantages of SOFCs include high energy conversion efficiency and big fuel flexibility. A typical SOFC single cell consists of three major components: a cathode, an anode and a ceramic electrolyte which is usually a solid oxygen ionic conductor. On the cathode side, O_2 is reduced and incorporated into the electrolyte defects, namely oxygen vacancies, resulting in the formation of O^{-2} ions. This process will be driven by the difference of chemical potential, which is established between two opposite electrodes, to O^{-2} ions move through the electrolyte to the anode where these can oxidize the fuels. All the electrons generated during the electrochemical oxidation process will be released to the external circuit for power generation. The look to high-performing and stable materials for Intermediate Temperature SOFCs (IT-SOFCs) is ongoing. Nickel-zirconia cermet is commonly used as fuel electrode; this material has excellent performance when using H2 or syngas fuels but results unsuitable for direct use of hydrocarbon fuels due to the inherent carbon deposition and the irreversible sulfur poisoning. In this sense, transition metal oxides with ABO_3-type perovskite structure are currently being researched as potential IT-SOFC anodes due to their mixed ionic-electronic conductivity, thermal expansion coefficients, and tolerance to sulphur.

Strontium titanate, STO, is one such material that has been found to be a versatile compound with excellent stability in reducing atmospheres (Sharma et al., 2024). However, it has a well know band-insulating electronic structure due to the formal $3d^0$ configuration of Ti^{+4}

Revista Tecnología y Ciencia
DOI: https://doi.org/10.33414/rtyc.53.95-108.2025 - ISSN 1666-6933

cations (Carballo-Córdova et al., 2019; Duan et al., 2017; Piskunov et al., 2004, 2005; Shein et al., 2005). In order to improve the electronic properties, it is possible to incorporate charge carriers trough oxygen vacancies (OV) or substitution of Sr^{+2} by a trivalent ion such as La^{+3} (Choi et al., 2014).

Several experimental studies have demonstrated the suitable electronic properties of La-doped STO, which are applicable to electrochemical devices such as SOFC (Burnat, Heel, Holzer, Kata, et al., 2012; Burnat, Heel, Holzer, Otal, et al., 2012; Cheng et al., 2021; Choi et al., 2014; Deshmukh et al., 2020; Fagg et al., 2001; Hashimoto et al., 2005; Savaniu & Irvine, 2011; Yurkiv et al., 2015; S. L. Zhang et al., 2014). In fact, Presto et al. (2018) point out that $La_{0.1}Sr_{0.9}TiO_3$ is presented as an alternative that optimizes electrochemical properties while maintaining structural stability.

By contrast, DFT calculations provides an important means of corroborating the hypotheses derived from experimental data. DFT enables the calculations of various parameters that are associated with different physical properties of the compound. These include geometric and optical properties, cell geometry, electronic band structure, the energy formation of defects and the density of states.

In the present study, first principles approach based on DFT within PBE-GGA approximation, as implemented in VASP code, was employed. Structural and electronic properties of pure $SrTiO_3$ and La-doped $SrTiO_3$ were investigated and compared in order to elucidate the impact of La-doping on the electrical properties of STO. In addition, a comprehensive Bader charge analysis was performed. To the best of our knowledge, this is the first report that employs a combination in procedures such as “Bader analysis” and “Small perturbation” analysis to achieve a more complete understanding of the electronic structure of stoichiometric and non-stoichiometric LST.

Computational details

DFT calculations were performed by using Vienna Ab Initio Simulation Package (VASP) (Kresse & Hafner, 1993). The properties have been calculated by using the projector-augmented-wave method (PAW) (Blöchl, 1994) developed by Blöchl to describe the ion-electron interactions. The kinetic energy cut off K_{max}= 640 eV was used for the plane-wave basis set during energy convergence. In self-consistent calculations, the total energy convergence was set to 0.01 eV. An exchange-correlation function Perdew-Burke Ernzerh (PBE) of generalized gradient approximation (GGA) (Perdew et al., 1996) was adopted for calculation of total ground state energy as well as for optimizing the structural cells internal parameters. A local Hubbard- U correction of 6.3 eV and 4 eV was also added to La and Ti atoms, respectively.

The Monkhorst-Pack’s k-points grid of 7×7×7 was used in the irreducible Brillouin zone (IBZ) for electronic structure calculations.

Compounds structures were described by using different supercell sizes: 2x2x2 and 4x2x2 supercells of the primitive cell. The 2x2x2 cell was used to study the properties of STO and LST-12 whereas 4x2x2 cell was used to study the compound with oxygen vacancies (V_o).

A series of lattice constants was set to obtain the total energy E and the corresponding primitive cell volume V. The lattice constants for the minimum total energy are the equilibrium lattice parameters, which was used to calculate the elastic constants. And then, the calculated E–V data was fitted to the Birch–Murnaghan equation of state (Birch, 1947).

For all the calculations, only ionic positions were relaxed during geometry optimization

Revista Tecnología y Ciencia
DOI: https://doi.org/10.33414/rtyc.53.95-108.2025 - ISSN 1666-6933

keeping the cell parameters fixed.

Charge Density Difference (CDD) was calculated by taking the difference of the charge density of the system and the isolated reference charge densities of atoms comprising the system according to equation (1). The CDD maps was plotted using VESTA software.

$$\Delta\rho = \rho_{LST} - \rho_{O} - \rho_{La} - \rho_{Sr} - \rho_{Ti} \quad (1)$$

Oxygen vacancy (O_V) defects were created by removing one oxygen atom from the supercell. The OV formation energy was computed according to equation (2) (Brown et al., 2018; Ha & Alexandrova, 2016; Su & Sun, 2015; L. Zhang et al., 2016).

$$\Delta E_{f,vac} = E_{O_V} - E_{perf} - \frac{1}{2}\mu_{O_2} \quad (2)$$

where E_{perf} is the total DFT energy of the defect-free supercell, E_{OV} is the total DFT energy of the supercell with a single defect, and μ_{O2} is the gas-phase chemical potential of molecular oxygen (μ_{O2}=−8.381 eV (−0.616 Ry))(Johnston et al., 2004; L. Zhang et al., 2016).

Results and discussion

Bulk properties

Simple cubic perovskite structure of type ABO_3, in the space group *Pm3m*, is the most common and stable phase of STO and LST-12 (Deshmukh et al., 2020; Hashimoto et al., 2005; Howard et al., 1989; Le et al., 2021). Figure 1 shows the 2x2x2 supercell of LST-12, in which, one Sr atom on site "A" has been replaced by La atom. The unit cell consists in 8 Ti (blue balls), 7 Sr (green balls), 1 La (brown balls) and 24 O (red balls) atoms and contains eight oxygen corner-sharing octahedra in a cubic arrangement.

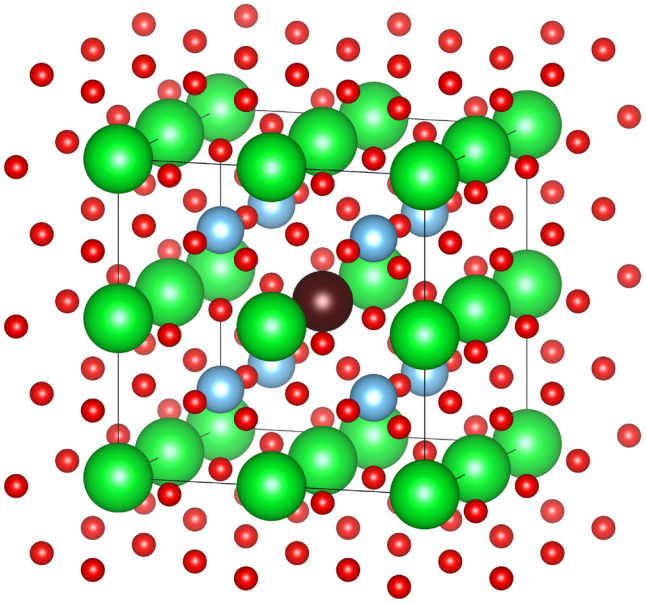

Fig. 1: 2x2x2 Supercell of the calculated structure of LST-12 (40-atom unit cell).

Revista Tecnología y Ciencia
DOI: https://doi.org/10.33414/rtyc.53.95-108.2025 - ISSN 1666-6933

At the first stage, the equilibrium states for non-magnetic STO and magnetic LST-12 compounds were determined by minimizing the total energy. Table 1 lists the lattice constants of both compounds. The calculated parameters are overestimated in respect to the experimental values, but the difference does not exceed 2%.

Phase	Lattice constant Å		B GPa	E_0 eV	dB/dP
	Calculated	Experimental			
LST-12	3.98	3.91	162	-301.64	4.20
STO	3.97	3.95	161	-299.21	4.21
R^2	0.99997				

Table 1: Calculated and experimental values of structural properties.

A graph of energy (*E*) versus volume (*V*) per formula unit for STO and LST-12 is given in figure 2. By fitting the corresponding *E-V* data to the Birch-Murnaghan equations of state it was obtained the isothermal bulk modulus B_0 and its pressure derivative dB/dP. The obtained values are listed in table 1. As observed, the elastic properties are remained practically unchanged in the phase doped with La. All obtained values are in good agreement with the experimental data (Adewale et al., 2020).

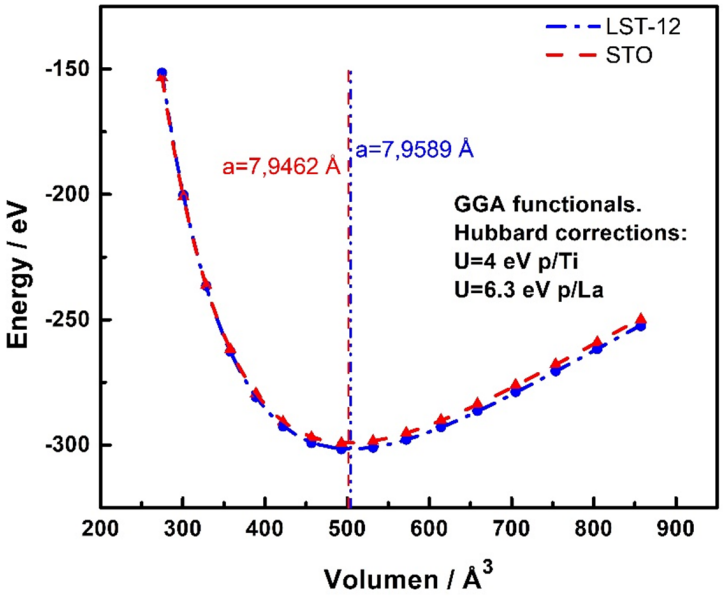

Fig. 2: Relations of dependence of the total energy on the lattice parameter for the magnetic phases of LST-12 and STO perovskites.

Electronic properties

Figure 3 shows the comparison of calculated densities of states (DOS) for STO and LST-12. In the ground state, STO is an insulator with a direct band-gap of 2.27 eV. This value is underestimated with respect to the reported experimental band-gap (3.75 eV) (Van Benthem et al., 2001). The LST-12 compound displays semi-metallic behaviour as the Fermi energy (E_F)

Revista Tecnología y Ciencia
DOI: https://doi.org/10.33414/rtyc.53.95-108.2025 - ISSN 1666-6933

level lies near the bottom in the conduction band (CB). This means the material is an electron charge carrier (n-type).

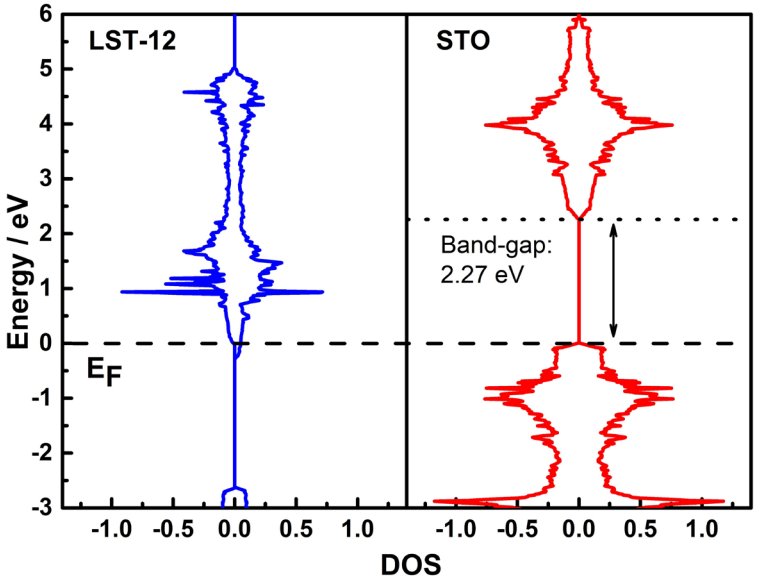

Fig. 3: The calculated total DOS for LST-12 and STO perovskites.

The contributions of each atom of LST-12 to the band structure lines cluster were analysed by computing the projected partial density of states. The total DOS and the band structure are presented in figure 4 (a) while the projected DOS are shown in figure 4 (b). The band structure has been plotted along the high symmetry points Γ-X-M-Γ-R-X-M of the Brillouin zone.

As these are displayed in figure 4 (b), the low-energy region around the gap is constituted by a valance band (VB) of mostly O-2p orbitals, while the conduction band (CB) is primarily characterized by Ti-3d orbitals.

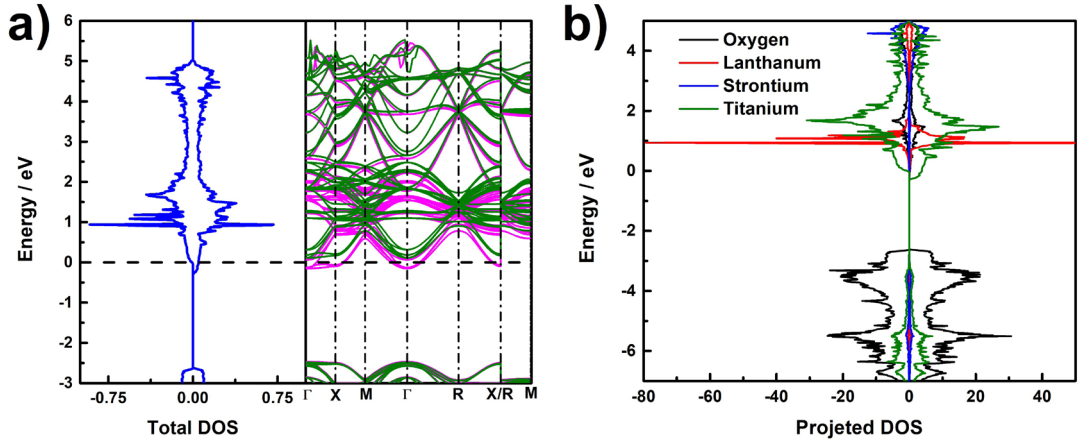

Fig. 4: Calculated total DOS with band structure (a) and (b) projected DOS for LST-12 perovskite.

Revista Tecnología y Ciencia
DOI: https://doi.org/10.33414/rtyc.53.95-108.2025 - ISSN 1666-6933

A magnetic behaviour was confirmed with different spin-up and spin-downs of DOS orbitals. Accordingly, the total magnetic moment calculated was 0.792 μ_B and over each atom results 0.001 μ_B for Sr, 0.023 μ_B for La, 0.124 μ_B for Ti and -0.01 μ_B for the oxygen.

Ti-ions in both STO and LST-12 present an octahedral coordination with six O-ligands surrounding them. This is confirmed in figure 5 in which the crystal field splitting is observed. The electrons in d-orbitals experience repulsion with the ligand electrons. This repulsion is stronger in the case of dx^2-y^2 and dz^2 orbitals as these point along the axes towards the direction of the ligand. Hence, they present higher energy than the average in the spherical crystal field. On the other hand, dxy, dyz and dxz orbitals experiment lower repulsions as they lie along the diagonals of the three planes. Therefore, these three orbitals have less energy than the average energy in the spherical crystal field. Thus, the 5-fold degenerate d-orbitals are divided into two energy levels: t_{2g}-set of three orbitals (dxy, dyz and dxz) with low energy and eg-set of two orbitals (dx^2-y^2 and dz^2) with high energy.

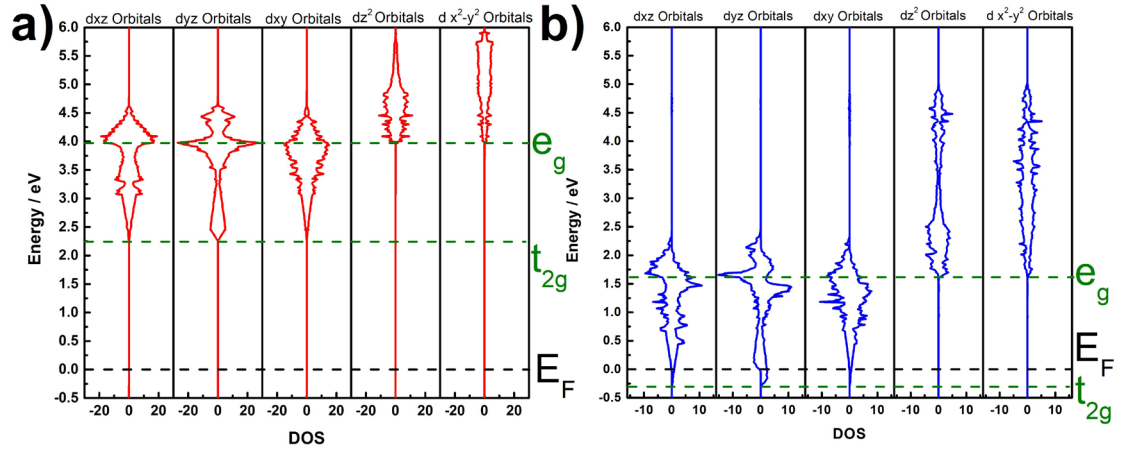

Fig. 5: The calculated DOS of Ti 3d states and their decomposition into the components t2g and eg for the (a) STO and (b) LST-12 perovskites.

Both compounds present different crystal splitting behaviour with different 10 Dq. Figure 5 (a) shows the projected DOS of Ti-3d in STO and figure 5 (b) shows the projected DOS of Ti-3d in LST-12. As it can be seen, the values of crystal field splitting 10 Dq are 1.73 eV and 1.9 eV in STO and LST-12, respectively. These values are underestimated respect the reported experimental values (Fan et al., 2019). La-doping in the A-site causes a slight increase in the splitting of the d orbitals, being more unfavourable to put electrons into higher energy sets of orbitals instead of pairing them up.

Bader charge analysis (Henkelman et al., 2006; Sanville et al., 2007; Tang et al., 2009) was used to analyse the charge density of the LST-12 phase and calculate the associated charge to each ion. This analysis allows to describe quantitatively the ionic/covalent character of the compound since under Bader's scheme the electron topology is characterized in terms of its critical points (CPs) which are defined as the zeros of the gradient of the electron density.

Revista Tecnología y Ciencia
DOI: https://doi.org/10.33414/rtyc.53.95-108.2025 - ISSN 1666-6933

Atom	Q_B (e)	Nominal ionic valences	VB (Å³)	δ (e/Å³)
Oxygen	-1.268 (Min)	-2	13.0694	0.097
	-1.1954 (Max)		12.6558	0.094
Strontium	1.5866 (Min)	+2	16.3651	0.097
	1.5979 (Max)		16.4074	0.097
Lanthanum	2.1922	+3	18.3964	0.119
Titanium	2.2078	+4	7.7331	0.284

Table 2. Parameters resulting from Bader analysis.

The Bader charge of Ti and O differs significantly from the formal ionic charges of ABO_3 perovskite: Ti^{4+} and O^{2-}. This can be explained by the significant overlap between the Ti 3d and O 2p orbitals, which results in a partial covalent O-Ti chemical bonding. In contrast, there is practically no bonding of O with Sr and La atoms. The charges of Sr and La remain close to the formal +2e and +3e respectively.

Figure 6 shows the CDD map on planes of interest. The positive CDD implies charge gain, while a negative CDD implies loss of electric charge. The colour reference ranges from blue in the negative extreme to red in the positive extreme.

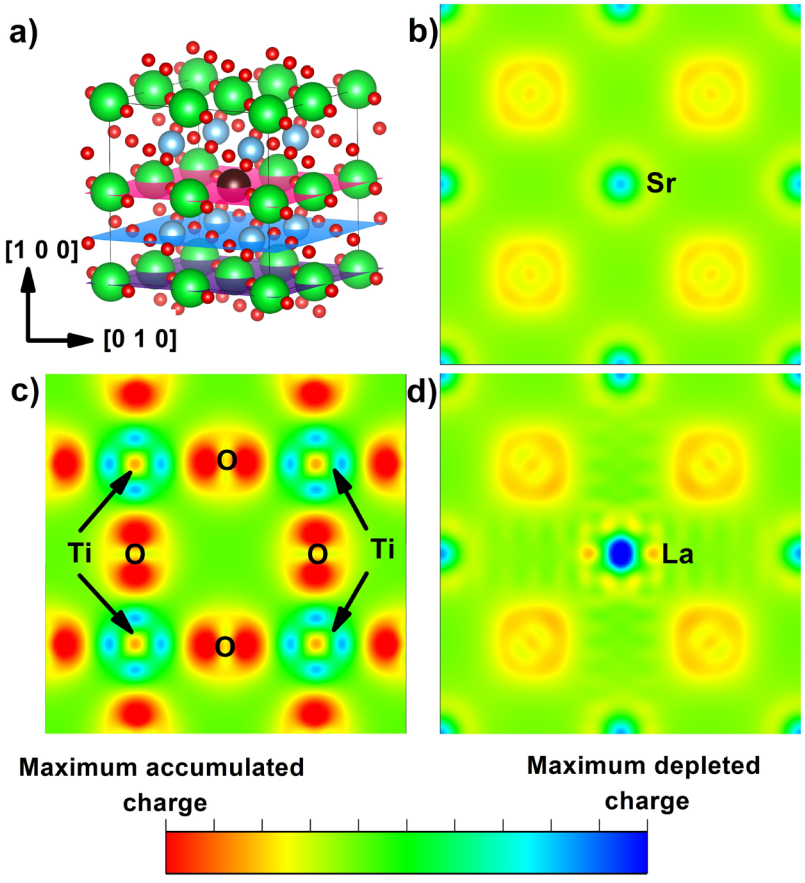

Fig. 6: Difference electron density plots for different cross sections; (a) structural unit of the cubic LST-12 perovskite crystal cross-sectioned by (1 0 0) plane, (b) CDD maps for Sr-O (1 0 0) cross sections, (c) CDD maps for Ti-O (1 0 0) cross sections and (d) CDD maps for La-O (1 0 0) cross sections

Revista Tecnología y Ciencia
DOI: https://doi.org/10.33414/rtyc.53.95-108.2025 - ISSN 1666-6933

Analysis of the CDD maps confirms the Ti-O covalent bonding effect mentioned above. Figure 6 (c) shows the concentration of the electronic density between Ti and O ions. In contrast, the CDD maps drawn for the AO-(1 0 0) cross sections (Figure 6 (b) and (d)) show no trace of the covalent bonding between the oxygen atom and Sr or La. The A cations on the AO-terminated surface demonstrate considerable polarization. Slight differences can be observed between the planes containing La and Sr. Figure 6 (b) shows that the electronic charge is spherically distributed around the sites occupied by O atoms, which is consistent with a perfect ionic bond. In contrast, in Figure 6 (d) it shows an asymmetric charge accumulation around oxygen and a greater depleted charge in the La position, due to the doping with these atoms.

When an extra electron is added to the material, in this case from the La donor, it will reside in two possible configurations. If the symmetry of the lattice is unbroken, the extra electron will be delocalized at the CB minimum. However, if the extra electron couples to the ions in the crystal a local distortion of the lattice is induced. This distortion produces an electric field that acts on the electron and generate a feedback mechanism that alters the energetics and dynamics of the charge carrier and may induces self-trapping. In consequence, a polaron is formed. The strong interaction of virtual phonons and electrons leads to problems in charge transport.

To study the possible formation of a quasiparticle, an intentional lattice deformation was introduced (Density Functional Perturbation Theory-DFPT) by changing the bond lengths of Ti-O (2.1 Å) and then performing a self-consistent calculation allowing the relaxation of ionic positions. The titanium charge values obtained from the Bader analysis, after the "small perturbation", indicate that the electron behaves as a free particle in a Fermi gas. The Bader charge value results around +2.21e for all Ti positions.

Oxygen vacancies

The oxygen vacancy formation energy in LST-12, calculated in our DFT study, yields 6.45 eV. This value is in good agreement with those reported for the undoped STO phase (Brown et al., 2018; L. Zhang et al., 2016). As can be seen in figure 7, the removal of one oxygen atom diminishes the symmetry of the crystal, leading to significant distortions in the crystal lattice due the rotation and deformation of TiO_6 octahedra. The Ti-O_V-Ti distance is increased to 4.02 Å while the Ti-O-Ti distances are slightly modified with respect to the distance in stoichiometric LST-12.

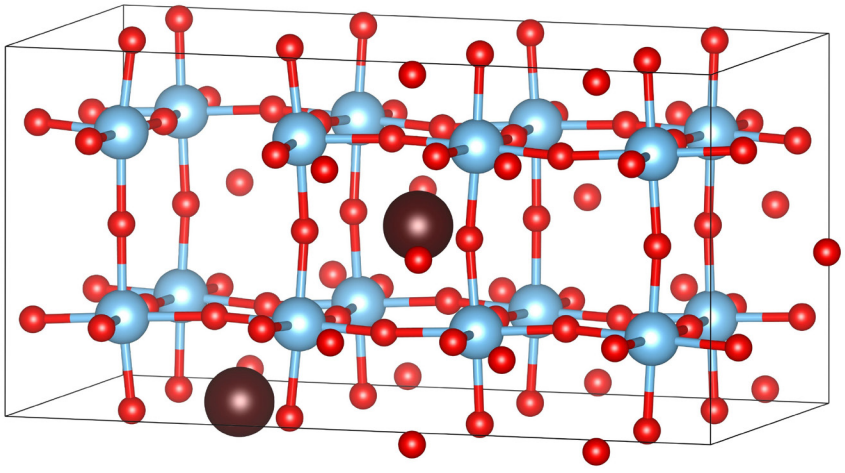

Fig. 7: Supercell 4x2x2 of the calculated structure of LST with one oxygen vacancy (79-atom unit cell)

Revista Tecnología y Ciencia
DOI: https://doi.org/10.33414/rtyc.53.95-108.2025 - ISSN 1666-6933

A similar behaviour has been observed by other authors (Souto-Casares et al., 2021; Winczewski et al., 2022; L. Zhang et al., 2016) in their calculation performed for STO phase.

Figure 8 shows the comparison between the total DOS and band structure of the stoichiometric LST-12 (Figure 9 a)) and defective $La_{0.12}Sr_{0.88}TiO_{3-\delta}$ (Figure 9 b)). As it can be exhibited, the main difference between the two calculations is the introduction of an electronic band at -0.6 eV below the Fermi level. The two electrons provided by the oxygen vacancy, mainly occupy the bands corresponding to the dz2 orbitals of titanium (Figure 9 c)).

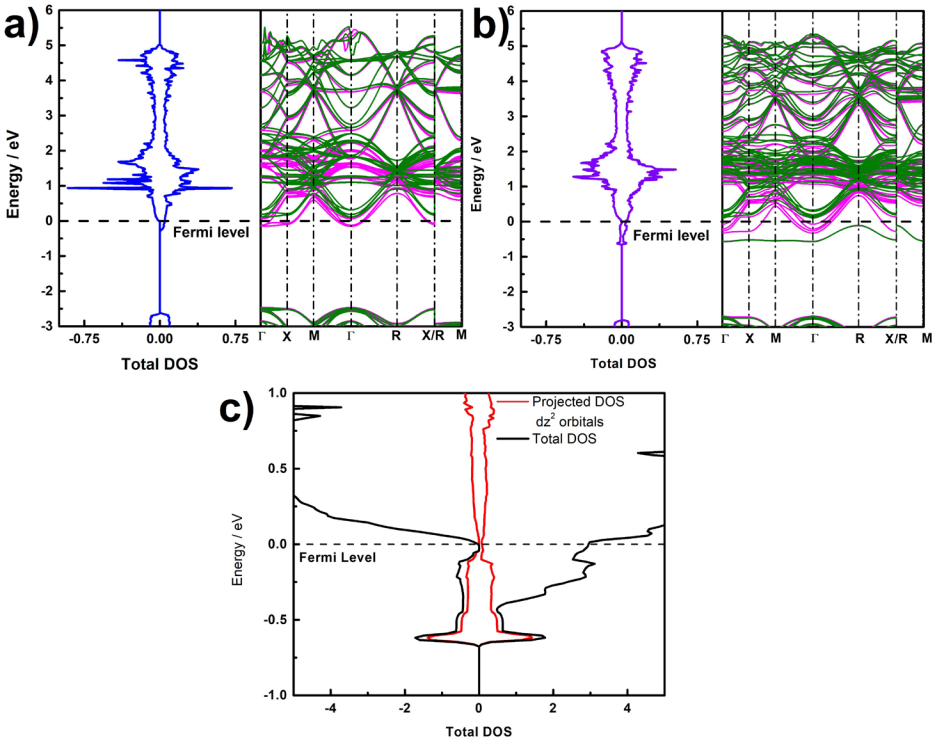

Fig. 8: Calculated DOS and band structure for (a) stoichiometric LST and (b) defective $La_{0.125}Sr_{0.875}TiO_{2.9375}$ and (c) calculated total DOS and projected DOS of Ti $3dz^2$ states.

The Bader analysis for the system with defects shows a decrease in the charge value of the Ti near to the vacancy site to +1.83e (Ti_4 and Ti_7 in figure 8) while the other Ti have a charge value around +2.2e which could be attributed to localized electrons forming Ti^{+3} polarons trapped around isolated oxygen vacancies.

Conclusions

First-principles calculations and Bader analysis were performed to examine the bulk and electronic properties of STO, LST and non-stoichiometric LST perovskite, as potential SOFC anodes. Calculations were performed with the generalized gradient approximation (GGA) taking into account the on-site Coulomb repulsive interaction (GGA + U). The results reveals that the calculated lattice constants of both compounds are in good agreement with experimental data and in previous reports available.

Revista Tecnología y Ciencia
DOI: https://doi.org/10.33414/rtyc.53.95-108.2025 - ISSN 1666-6933

Regarding the electronic properties, it was demonstrated that when STO is doped with a donor such as La, it exhibits metallic-like behavior. In addition, LST displays magnetic properties with a total magnetic moment of ~0.8 μB, whereas STO present non-magnetic behavior. Also, it was possible to observe the crystal field splitting by Ti-projected DOS. The 10 Dq yielded 1.73 eV and 1.9 eV for STO and LST, respectively. Bader's analysis facilitated an understanding of the nature of the chemical bonds in the compound, revealing a partially Ti-O covalent bond and a strong ionic character in Sr and La, which was confirmed by CDD maps. Additionally, polaronic modes of conduction were discarded by means of an intentional lattice deformation and subsequent ionic relaxation.

Finally, the formation energy of a vacancy was calculated, and the distortion of the crystalline structure was verified. A lower symmetry was observed due to the rotation of the octahedra TiO_6. A notable decrease in the Bader charge value was evident in the Ti region close to the vacancy, which could be attributed to the formation of Ti^{+3} polarons.

The main contribution of this work was relating the electronic and structural properties at the atomic level to the expected performance as an SOFC anode. It was observed that doping with La provides the material with adequate characteristics for hydrogen catalysis and good electronic conductivity properties.

Acknowledgments

The authors thank to Comisión Nacional de Energía Atómica (CNEA) and Consejo Nacional de Investigaciones Científicas y Técnicas (CONICET). Additionally, we would like to acknowledge the Dr Veronica Vildosola and María Andrea Barral for their technical assistance in the development of the calculations and for allowing access to the computational resources.

Revista Tecnología y Ciencia
DOI: https://doi.org/10.33414/rtyc.53.95-108.2025 - ISSN 1666-6933

Reference

Adewale, A. A., Chik, A., & Zaki, R. M. (2020). Structural, electronic and thermoelectric properties of SrTiO3 ceramic doped by lanthanum using first principles. *IOP Conference Series: Materials Science and Engineering*, *957*(1), 0–10. https://doi.org/10.1088/1757-899X/957/1/012008

Birch, F. (1947). Finite elastic strain of cubic crystals. *Physical Review*, *71*(11), 809–824. https://doi.org/10.1103/PhysRev.71.809

Blöchl, P. E. (1994). Projector augmented-wave method. *Physical Review B*, *50*(24), 17953–17979. https://doi.org/10.1103/PhysRevB.50.17953

Brown, J. J., Ke, Z., Geng, W., & Page, A. J. (2018). Oxygen Vacancy Defect Migration in Titanate Perovskite Surfaces: Effect of the A-Site Cations. *Journal of Physical Chemistry C*, *122*(26), 14590–14597. https://doi.org/10.1021/acs.jpcc.8b03322

Burnat, D., Heel, A., Holzer, L., Kata, D., Lis, J., & Graule, T. (2012). Synthesis and performance of A-site deficient lanthanum-doped strontium titanate by nanoparticle based spray pyrolysis. *Journal of Power Sources*, *201*, 26–36. https://doi.org/10.1016/j.jpowsour.2011.10.088

Burnat, D., Heel, A., Holzer, L., Otal, E., Kata, D., & Graule, T. (2012). On the chemical interaction of nanoscale lanthanum doped strontium titanates with common scandium and yttrium stabilized electrolyte materials. *International Journal of Hydrogen Energy*, *37*(23), 18326–18341. https://doi.org/10.1016/j.ijhydene.2012.09.022

Carballo-Córdova, D. A., Ochoa-Lara, M. T., Olive-Méndez, S. F., & Espinosa-Magaña, F. (2019). First-principles calculations and Bader analysis of oxygen-deficient induced magnetism in cubic BaTiO3−x and SrTiO3−x. *Philosophical Magazine*, *99*(2), 181–197. https://doi.org/10.1080/14786435.2018.1535722

Cheng, J., Gong, J., Yue, S., Jiang, Y., Hou, X., Ma, J., Yao, Y., & Jiang, C. (2021). Electrochemical investigation of La0.4Sr0.6TiO3 synthesized in air for SOFC application. *Journal of Applied Electrochemistry*, *51*(8), 1175–1188. https://doi.org/10.1007/s10800-021-01568-8

Choi, M., Posadas, A. B., Rodriguez, C. A., O'Hara, A., Seinige, H., Kellock, A. J., Frank, M. M., Tsoi, M., Zollner, S., Narayanan, V., & Demkov, A. A. (2014). Structural, optical, and electrical properties of strained La-doped SrTiO3 films. *Journal of Applied Physics*, *116*(4). https://doi.org/10.1063/1.4891225

Deshmukh V., Nagaswarupa H., Ravikumar C., Anil Kumar M., Shashi Shekhar T., A. M. H. (2020). Lanthanum doped strontium titanate nanomaterial for photocatalytic and supercapacitor applications. *Asian Journal of Chemistry*, *32*(8), 2013–2020.

Duan, Y., Ohodnicki, P., Chorpening, B., & Hackett, G. (2017). Electronic structural, optical and phonon lattice dynamical properties of pure- and La-doped SrTiO3: An ab initio thermodynamics study. *Journal of Solid State Chemistry*, *256*(August), 239–251. https://doi.org/10.1016/j.jssc.2017.09.016

Fagg, D. P., Kharton, V. V., Kovalevsky, A. V., Viskup, A. P., Naumovich, E. N., & Frade, J. R. (2001). The stability and mixed conductivity in La and Fe doped SrTiO3 in the search for potential SOFC anode materials. *Journal of the European Ceramic Society*, *21*(10–11), 1831–1835. https://doi.org/10.1016/S0955-2219(01)00125-X

Fan, W., Song, Y., Bi, J., Pei, Y., Zhang, R., & Cao, Y. (2019). Evolution of element-specific electronic structures in alkaline titanates. *AIP Advances*, *9*(6), 1–6. https://doi.org/10.1063/1.5109588

Revista Tecnología y Ciencia
DOI: https://doi.org/10.33414/rtyc.53.95-108.2025 - ISSN 1666-6933

Ha, M.-A., & Alexandrova, A. N. (2016). Oxygen Vacancies of Anatase(101): Extreme Sensitivity to the Density Functional Theory Method. *Journal of Chemical Theory and Computation*, *12*(6), 2889–2895. https://doi.org/10.1021/acs.jctc.6b00095

Hashimoto, S., Kindermann, L., Poulsen, F. W., & Mogensen, M. (2005). A study on the structural and electrical properties of lanthanum-doped strontium titanate prepared in air. *Journal of Alloys and Compounds*, *397*(1–2), 245–249. https://doi.org/10.1016/j.jallcom.2004.11.066

Henkelman, G., Arnaldsson, A., & Jónsson, H. (2006). A fast and robust algorithm for Bader decomposition of charge density. *Computational Materials Science*, *36*(3), 354–360. https://doi.org/10.1016/j.commatsci.2005.04.010

Howard, S. A., Yau, J. K., & Anderson, H. U. (1989). Structural characteristics of Sr1-xLaxTi 3+δ as a function of oxygen partial pressure at 1400°C. *Journal of Applied Physics*, *65*(4), 1492–1498. https://doi.org/10.1063/1.342963

Johnston, K., Castell, M. R., Paxton, A. T., & Finnis, M. W. (2004). SrTiO3(001)(2×1) reconstructions: First-principles calculations of surface energy and atomic structure compared with scanning tunneling microscopy images. *Physical Review B - Condensed Matter and Materials Physics*, *70*(8), 1–12. https://doi.org/10.1103/PhysRevB.70.085415

Kresse, G., & Hafner, J. (1993). Ab initio molecular dynamics for liquid metals. *Physical Review B*, *47*(1), 558–561. https://doi.org/10.1103/PhysRevB.47.558

Le, M., Vo, N., Le, Q., Tran, V. A., & Phan, T. Q. (2021). *Sr 1 − x La x TiO 3 Nanocubes toward the Photodegradation of 2-Naphthol under Artificial Solar Light*.

Perdew, J. P., Burke, K., & Ernzerhof, M. (1996). Generalized gradient approximation made simple. *Physical Review Letters*, *77*(18), 3865–3868. https://doi.org/10.1103/PhysRevLett.77.3865

Piskunov, S., Heifets, E., Eglitis, R. I., & Borstel, G. (2004). Bulk properties and electronic structure of SrTiO3, BaTiO 3, PbTiO3 perovskites: An ab initio HF/DFT study. *Computational Materials Science*, *29*(2), 165–178. https://doi.org/10.1016/j.commatsci.2003.08.036

Piskunov, S., Kotomin, E. A., Heifets, E., Maier, J., Eglitis, R. I., & Borstel, G. (2005). Hybrid DFT calculations of the atomic and electronic structure for ABO 3 perovskite (0 0 1) surfaces. *Surface Science*, *575*(1–2), 75–88. https://doi.org/10.1016/j.susc.2004.11.008

Presto, S., Barbucci, A., Carpanese, M., Han, F., Costa, R., & Viviani, M. (2018). Application of La-Doped SrTiO3 in Advanced Metal-Supported Solid Oxide Fuel Cells. *Crystals*, *8*(3), 134. https://doi.org/10.3390/cryst8030134

Sanville, E., Kenny, S. D., Smith, R., & Henkelman, G. (2007). Improved grid-based algorithm for Bader charge allocation. *Journal of Computational Chemistry*, *28*(5), 899–908. https://doi.org/10.1002/jcc.20575

Savaniu, C. D., & Irvine, J. T. S. (2011). La-doped SrTiO3 as anode material for IT-SOFC. *Solid State Ionics*, *192*(1), 491–493. https://doi.org/10.1016/j.ssi.2010.02.010

Sharma, U., Pawar, V., & Singh, P. (2024). Charge particle dynamics and electrochemical behaviour of SrTiO3-δ as anode material for IT-SOFC applications. *International Journal of Hydrogen Energy*, *52*, 1278–1289. https://doi.org/10.1016/j.ijhydene.2023.11.007

Shein, I. R., Shein, K. I., Kozhevnikov, V. L., & Ivanovskiĭ, A. L. (2005). Band structure and the magnetic and elastic properties of SrFeO3 and LaFeO3 perovskites. *Physics of the Solid State*, *47*(11), 2082–2088. https://doi.org/10.1134/1.2131149

Revista Tecnología y Ciencia
DOI: https://doi.org/10.33414/rtyc.53.95-108.2025 - ISSN 1666-6933

Souto-Casares, J., Spaldin, N. A., & Ederer, C. (2021). Oxygen vacancies in strontium titanate: A DF +DMFT study. *Physical Review Research, 3*(2), 023027. https://doi.org/10.1103/PhysRevResearch.3.023027

Su, H. Y., & Sun, K. (2015). DFT study of the stability of oxygen vacancy in cubic ABO3 perovskites. *Journal of Materials Science, 50*(4), 1701–1709. https://doi.org/10.1007/s10853-014-8731-0

Tang, W., Sanville, E., & Henkelman, G. (2009). A grid-based Bader analysis algorithm without lattice bias. *Journal of Physics: Condensed Matter, 21*(8), 084204. https://doi.org/10.1088/0953-8984/21/8/084204

Van Benthem, K., Elsässer, C., & French, R. H. (2001). Bulk electronic structure of SrTiO3: Experiment and theory. *Journal of Applied Physics, 90*(12), 6156–6164. https://doi.org/10.1063/1.1415766

Winczewski, S., Dziedzic, J., Miruszewski, T., Rybicki, J., & Gazda, M. (2022). Properties of Oxygen Vacancy and Hydrogen Interstitial Defects in Strontium Titanate: DFT + Ud,pCalculations. *Journal of Physical Chemistry C, 126*(43), 18439–18465. https://doi.org/10.1021/acs.jpcc.2c04681

Yurkiv, V., Constantin, G., Hornes, A., Gondolini, A., Mercadelli, E., Sanson, A., Dessemond, L., & Costa, R. (2015). Towards understanding surface chemistry and electrochemistry of La0.1Sr0.9TiO3-α based solid oxide fuel cell anodes. *Journal of Power Sources, 287*, 58–67. https://doi.org/10.1016/j.jpowsour.2015.04.039

Zhang, L., Liu, B., Zhuang, H., Kent, P. R. C., Cooper, V. R., Ganesh, P., & Xu, H. (2016). Oxygen vacancy diffusion in bulk SrTiO3 from density functional theory calculations. *Computational Materials Science, 118*, 309–315. https://doi.org/10.1016/j.commatsci.2016.02.041

Zhang, S. L., Li, C. X., & Li, C. J. (2014). Chemical compatibility and properties of suspension plasma-sprayed SrTiO3-based anodes for intermediate-temperature solid oxide fuel cells. *Journal of Power Sources, 264*, 195–205. https://doi.org/10.1016/j.jpowsour.2014.04.094

Contribución de los Autores

	Colaboración Académica													
Nombres y Apellidos del autor	1	2	3	4	5	6	7	8	9	10	11	12	13	14
Ernesto Tagarelli		x	x		x	x	x	x	x	x	x			x
Jesús Vega-Castillo						x							x	x
Mariela Ortíz						x							x	x
Alejandra Montenegro-Hernandez	x	x		x		x		x	x			x	x	x

1-Administración del proyecto, **2-**Adquisición de fondos, **3-**Análisis formal, **4-**Conceptualización, **5-**Curaduría de datos, **6-**Escritura - revisión y edición, **7-**Investigación, **8-**Metodología, **9-**Recursos, **10-**Redacción - borrador original, **11-**Software, **12-**Supervisión, **13-**Validación, **14-**Visualización.